Received 13 February 2022; revised 29 March 2022; accepted 6 April 2022. Date of publication 12 April 2022; date of current version 25 April 2022.

Digital Object Identifier 10.1109/OJAP.2022.3166633

Dimension and Sampling of the Near-Field and Its Intensity Over Curves

GIOVANNI LEONE (Member, IEEE), RAFFAELE MORETTA (Member, IEEE), AND ROCCO PIERRI

Dipartimento di Ingegneria, Università degli Studi della Campania "Luigi Vanvitelli," 81031 Aversa, Italy

CORRESPONDING AUTHOR: R. MORETTA (e-mail: raffaele.moretta@unicampania.it)

This work was supported by the Italian Ministry of University and Research through PRIN 2017 Program.

ABSTRACT The paper addresses the question of efficiently sampling the near field and its intensity over an arbitrary curved line. It aims at finding the minimum number of measurements and their position for discretizing the near field and its square amplitude without loss of information and follows a common approach for both the radiation operator and the correspondent lifting operator. A scalar geometry is examined for both electric and magnetic current sources.

At first, the singular values of the radiation / lifting operator are evaluated by an asymptotic approach and a change of variables which lead to an operator with a widely investigated spectrum. As the number of relevant singular values is available in closed form, the dimensions of the near field and its intensity over the curve are found. Next, starting from a sampling expansion of the pertinent left singular functions, a non-redundant sampling representation of the near field and its square amplitude is provided. Some numerical results confirm the analysis. The results may be of great interest especially in antenna testing by near field data (both standard and phaseless) with an unconventional field scanning system as, for instance, an UAV mounted probe.

INDEX TERMS Electromagnetic inverse problems, near field sampling, singular value decomposition.

I. INTRODUCTION

FIELD sampling is a relevant research topic arising in antenna characterization [1]–[5], inverse source [6]–[9], imaging problems [10]–[14], etc. In particular, sampling methods employing a non-redundant number of field measurements are gaining an ever-increasing interest since they allow to save time in the field probing which is dominated by the mechanical scanning. In this framework, the determination of the minimum number of measurements to avoid loss of information in the field discretization is a relevant task both from the theoretical and the applicative points of view.

Here, the attention is focused on the sampling of the field radiated by an antenna. The latter is related to the actual or equivalent source current J_i by the linear model $E = T_i J_i$ where T_i stands for the radiation operator.

For establishing the minimum number of measurements required to correctly sample the radiated field, the *number of degrees of freedom* (NDF) must be computed [15], [16]. The latter provides the dimension of the subspace of the currents that can be stably reconstructed and, at the same time, the dimension of the subspace of the fields that allows representing the radiated field with good accuracy. Accordingly, the NDF represents the "essential" dimension of the field space and it can be evaluated by determining the number of significant singular values of the radiation operator [17], [18].

Once the minimum number of field measurements has been found, another important task is to find their location. Classical sampling techniques for the case of planar, cylindrical and spherical scanning were introduced respectively in [19], [20], and [21]. According to such techniques, in the case of planar scanning the radiated field must be collected with a uniform sampling step equal to the half-wavelength. Instead, in the case of spherical scanning, the field must be observed along the azimuth and elevation coordinates in a number of points proportional to the radius of the minimum sphere enclosing the source.

Despite their simplicity, these techniques do not consider the source shape. Hence, they may require collecting a number of measurements considerably higher than the NDF. To reduce the field measurements, other sampling strategies have been conceived [22]–[33]. Among these, the

one proposed by Prof. Bucci *et al.* [23] is of great interest since it avoids loss of information with a number of field samples proximal to the NDF and provides a closed-form expression to compute the location of the sampling points. Such sampling criterion relies on the study of the local bandwidth of the so-called reduced field and it can be applied to sample the field radiated by a source enclosed within an ellipsoid. Moreover, also planar disk and spherical sources can be considered since they can be seen as particular cases of an ellipsoidal source.

Recently, a discretization of the radiation operator that returns a discrete model with the same singular values of the continuous one has been proposed in [34], [35]. In these papers, a warping transformation is exploited to recast the kernel of the related eigenvalues problem as a convolution and bandlimited function. Then, the continuous model is discretized by applying the sampling theory approach exposed in [36] and a sampling representation of the near field that employs a number of samples essentially equal to the NDF is derived.

Despite the approaches in [23] and [35] are different each other, in the case of 2D strip sources they return the same non-uniform arrangement of the sampling points along the observation domain.

In this paper, the sampling approach proposed in [35] for a 2D magnetic current strip observed in near zone over a line parallel to the source is generalized to a large class of smooth curves, both in the case of magnetic or electric current strips. The consequent flexibility makes our sampling scheme suitable also for offset configurations (i.e., geometries where the observation curve is not centered with respect to the source location) [37], and unconventional observation curves as the trajectory followed by an UAV-based system for the in-situ testing of radiating systems [38]–[40].

In the second part of the paper, the approach developed for the near-field is extended to its intensity, i.e., the square modulus. This can be of fundamental importance in source reconstruction problems and antenna testing since, especially at high frequencies, the phase of the near field cannot be accurately measured. Accordingly, it arises the need of addressing a phase retrieval problem to recover the source current or the far field pattern from only intensity measurements of the near field [41]–[45]. In this framework, the "essential" dimension of the field intensity plays a key role. On one hand, it provides the minimum number of phaseless measurements required to not lose information in the sampling of the near field intensity. On the other, it impacts on the presence of local minima in the optimization algorithm solving the correspondent phase retrieval problem. In fact, the higher the "essential" dimension of the field intensity, the lower the occurrence of local minima [46], [47].

The "essential" dimension of the field intensity and the samples positions are found by extending the study over the radiation operator to the correspondent lifting operator [48].

Therefore, the paper is organized as follows. In Section II, the mathematical formulation of the problem for the near field case in a 2D geometry for both magnetic and electric currents is provided. In Section III, asymptotic approximations of the operators involved in the computation of the singular values are discussed. In Section IV, the dimension of the near field and a sampling strategy is provided. In Section V, numerical examples corroborating the analytical results are shown. Finally, Section VII provides the extension of the developed approach to the near field intensity.

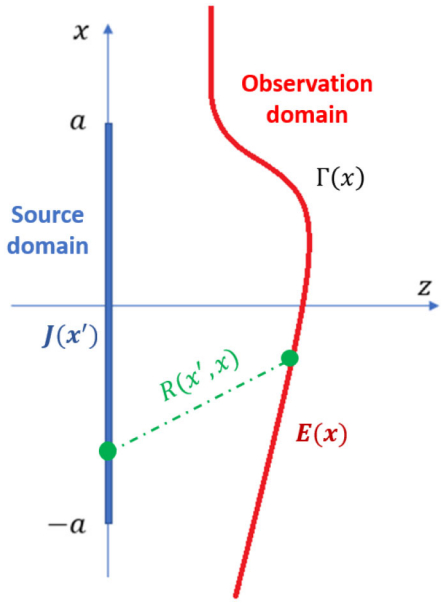

FIGURE 1. Geometry of the problem.

II. MATHEMATICAL FORMULATION

Consider the 2D geometry invariant along the y-axis depicted in Fig. 1.

An electric or magnetic density current is directed along the $\boldsymbol{y}-$axis and supported over the interval $SD = [-a, a]$. Hence, it can be expressed as

$$\overline{J}_i(x') = J_i(x')\ \hat{y} \tag{1}$$

where the subscript $i \in \{e, m\}$ distinguishes the electric case by the magnetic one.

The electric field corresponding to $\overline{J}_e(x')$ has only a component directed as the density current; instead, the electric field radiated by $\overline{J}_m(x')$ has two components: one directed along the $x-$axis, and the other along the $z-$axis. The tangential component E of the electric field is observed in near zone over a smooth curve $\boldsymbol{\Gamma}(x) = (x, z(x))$ with $x \in OD = [x_{min}, x_{max}]$. Accordingly, E is given by

$$E(x) = T_i\ J_i(x') \tag{2}$$

where

$$T_i : J_i \in L^2(SD) \rightarrow E \in L^2(OD) \tag{3}$$

with $L^2(SD)$ and $L^2(OD)$ denoting the space of square integrable functions defined over SD and OD, respectively. For the geometry at hand, the radiation operator T_i can be explicitly written as

$$T_i J_i = \int_{-a}^{+a} g_i(x', x) J_i(x') dx' \tag{4}$$

where the Green function $g_i(x', x)$ is given by

$$g_i(x', x) = \begin{cases} -\zeta \sqrt{\frac{\beta}{8\pi}} e^{j\frac{\pi}{4}} \frac{1}{\sqrt{R(x', x)}} e^{-j\beta R(x', x)} & for\ i = e \\ -\sqrt{\frac{\beta}{8\pi}} e^{j\ \frac{\pi}{4}} \frac{z(x)}{R^{\frac{3}{2}}(x', x)} e^{-j\beta R(x', x)} & for\ i = m \end{cases} \tag{5}$$

with β denoting the wavenumber, ζ the impedance of the medium, and $R(x', x) = \sqrt{(x - x')^2 + z^2(x)}$.

Since the radiation operator is linear, its singular system $\{\sigma_n,\ v_n, u_n\}$ can be introduced where

- $\{\sigma_n\}$ are the singular values ordered in a non-decreasing way,
- $\{u_n\}$ and $\{v_n\}$ are the left and right singular functions spanning the current and the field spaces, respectively.

The singular functions are linked each other by

$$T_i u_n = \sigma_n v_n \qquad T_i^\dagger v_n = \sigma_n u_n \tag{6}$$

with $T_i^\dagger$ being the adjoint operator. In this paper, a weighted adjoint operator is exploited; accordingly, $T_i^\dagger$ is defined as

$$T_i^\dagger E = \int_{x_{min}}^{x_{max}} w_i(x', x) g_i^*(x', x) E(x) \left\| \mathbf{\Gamma}'(x) \right\| dx \tag{7}$$

where

- $w_i(x', x)$ is a positive and real function acting as a weight,
- $\|\mathbf{\Gamma}'(x)\| = \sqrt{1 + [z'(x)]^2}$ is the norm of the first derivative of $\mathbf{\Gamma}(x)$.

In light of (6), the following shifted eigenvalues problem can be written

$$T_i T_i^\dagger v_n = \sigma_n^2 v_n \tag{8}$$

from which is evident that the eigenvalues of the auxiliary operator $T_i T_i^\dagger$ are the square of the singular values of $T_i^\dagger$.

The singular values decomposition represents a key mathematical tool to achieve the main goals of the paper which consist in

1. finding the NDF of the near field,
2. providing a sampling representation of the near field that employs a number of field samples equal to the NDF.

As concerns the first task, the NDF are given by the number of significant singular values of the radiation operator. In particular, since the kernel of T_i (i.e., the Green function g_i) is an entire function of exponential type, its singular values exhibit an abrupt decay in correspondence of a critical index M [49], [50]. The latter delimits the most relevant singular values of T_i and provides an evaluation of the NDF, i.e., the dimension of the near field.

It is worth noting that the presence of a real and positive weight function in the adjoint operator definition modifies only the dynamics of the singular values but not the critical index at which they abruptly decay [51]. Accordingly, the number of relevant singular values does not change by introducing $w_i(x', x)$ in the adjoint operator definition and, consequently, the NDF can be found by solving the weighted eigenvalue problem (8).

With regard to the second task, it is addressed by providing a sampling representation of the left singular functions $\{v_n\}$ efficient in terms of the required field samples. Then, recalling that the radiated field E can be expressed in terms of the left singular functions by the equation $E = \sum_n c_n v_n$, the correspondent sampling representation of the radiated field efficient is found.

III. STUDY OF THE OPERATOR $T_i T_i^\dagger$

In this section the operator $T_i T_i^\dagger$ is considered and recast as a convolution and bandlimited operator whose eigenvalues are known in closed form.

Let us rewrite the eigenvalues problem (8) in the following explicit form

$$\int_{x_{min}}^{x_{max}} K_i(x_o, x) v_n(x) dx = \sigma_n^2 v_n(x_o) \tag{9}$$

with $K_i(x_o, x)$ denoting the pertinent kernel function. The latter is given by

$$K_i(x_o, x) = \left\| \mathbf{\Gamma}'(x) \right\| \int_{-a}^{+a} w_i(x', x) A_i(x', x_o, x) e^{-j\beta a\ \Phi(x',\ x_o,\ x)} dx' \tag{10}$$

where

$$A_i(x', x_o, x) = \begin{cases} \frac{\zeta^2 \beta}{8\pi \sqrt{R(x', x_o) R(x', x)}} & for\ i = e \\ \frac{\beta z(x) z(x_o)}{8\pi R^{\frac{3}{2}}(x', x_o)\ R^{\frac{3}{2}}(x', x)} & for\ i = m \end{cases} \tag{11}$$

and

$$\Phi(x', x_o, x) = \frac{1}{a}\left[R(x', x_o) - R(x', x)\right] \tag{12}$$

For $x_o = x$, it results that $\Phi = 0$; accordingly, the integral (10) can be evaluated by exploiting the integration by parts method.

For $x_o \neq x$, if the hypothesis $\beta a \gg 1$ is fulfilled, the kernel function can be asymptotically evaluated. Since the choice of the asymptotic technique is related to the presence of stationary points in the phase function Φ, the solution of the stationary condition $\Phi'(x', x, x_o) = 0$ with respect to variable x' must be discussed. This is done in Appendix A where a condition on the observation curve for the absence of stationary points is provided. In particular, in such Appendix it is shown that if all the possible straight lines linking two generic points of the observation curve do not intersect with the source then equation $\Phi'(x', x, x_o) = 0$ does not admit solution $\forall x_o \neq x$. When this happens, the integral (10) can be asymptotically evaluated by considering only the contributions of the endpoints $x' = a$ and $x' = -a$. More in detail, after the application of the integration by

parts method, $\forall x_o \neq x$ the kernel function $K_i(x_o, x)$ can be written as

$$K_i(x_o,x) = -\frac{1}{j\beta a}\left\|\boldsymbol{\Gamma}'(x)\right\| \begin{pmatrix} w_i(x',x)\frac{A_i(x',x_o,x)}{\Phi'(x',x_o,x)}e^{-j\beta a\ \Phi(x',x_o,x)}\Big|_{x'=a}^{x'=a} - \\ \int_{-a}^{a}\frac{d}{dx'}\left(w_i(x',x)\frac{A_i(x',x_o,x)}{\Phi'(x',x_o,x)}\right)e^{-j\beta a\ \Phi}dx' \end{pmatrix} \tag{13}$$

By the Riemann - Lebesgue lemma, the integral in (13) tends to zero; hence, the kernel function can be approximated only with the first term. The latter is not of convolution type (i.e., it does not depend on the difference $x_o - x$); accordingly, an analytical evaluation of the eigenvalues of $T_i T_i^{\dagger}$ is a very difficult task. To recast $K_i(x_o, x)$ in a form more similar to a convolution kernel, it can be first approximated as

$$\begin{aligned} &K_i(x_o,x) \\ &\approx -\frac{1}{j\beta a}\ \left|\left|\ \boldsymbol{\Gamma}'(x)\right|\right|\ e^{-j\ \frac{\beta a}{2}\ (\Phi(a,x_o,x)+\Phi(-a,x_o,x))} \\ &\begin{pmatrix} \frac{w_i(a,x)\ A_i(a,x_o,x)}{\Phi'(a,x_o,x)}e^{j\ \frac{\beta a}{2}\ (\Phi(-a,x_o,x)-\ \Phi(a,x_o,x))} - \\ \frac{w_i(-a,x)A_i(-a,x_o,x)}{\Phi'(-a,x_o,x)}e^{-j\ \frac{\beta a}{2}\ (\Phi(-a,x_o,x)-\ \Phi(a,x_o,x))} \end{pmatrix} \end{aligned} \tag{14}$$

Then, the elliptic coordinates

$$\eta(x) = \frac{R(-a,x) - R(a,x)}{2a} \tag{15}$$

$$\gamma(x) = \frac{R(-a,x) + R(a,x)}{2a} \tag{16}$$

can be introduced to recast the kernel function as

$$K_i(\eta_o,\eta) \approx -\frac{1}{j\beta a}\ \left\|\boldsymbol{\Gamma}'(x(\eta))\right\|\frac{dx}{d\eta}e^{-j\ \beta a\ (\gamma(\eta_o)-\gamma(\eta))} \begin{pmatrix} w_i(a,\eta)\frac{A_i(a,\eta_o,\eta)}{\Phi'(a,\eta_o,\eta)}e^{j\beta a(\eta_o-\eta)} - \\ w_i(-a,\eta)\frac{A_i(-a,\eta_o,\eta)}{\Phi'(-a,\eta_o,\eta)}e^{-j\beta a(\eta_o-\eta)} \end{pmatrix} \tag{17}$$

where $dx/d\eta$ is the Jacobian term arising from the change of the integration variable in the eigenvalue problem (9).

In the new couple of variables $\eta_o = \eta(x_o)$ and $\eta = \eta(x)$, the exponential terms in (17) depend on the difference $(\eta_o - \eta)$; instead, the amplitude terms are still not convolution. However, in all the cases where A_i/Φ' can be approximated as the product between a function depending $(\eta - \eta_o)$ and a function depending on η, the kernel function $K_i(\eta_o, \eta)$ can be recast in a convolution form by choosing the weight function in such a way to compensate all the amplitude terms depending only on the variable η. More in detail, when the observation domain is not significantly larger than the source domain, the numerator and the denominator of A_i/Φ' can be approximated with respect to η_o in a Taylor series stopped at the first non-zero term, i.e.,

$$\frac{A_i(\pm a,\eta_o,\eta)}{\Phi'(\pm a,\eta_o,\eta)} \approx \frac{A_i(\pm a,\eta_o,\eta_o)}{\frac{d\Phi'(\pm a,\eta_o,\eta)}{dx}\frac{dx}{d\eta_o}|_{\eta_o=\eta}(\eta_o-\eta)} \tag{18}$$

Then, the kernel function can be written as

$$K_i(\eta_o,\eta) \approx -\frac{1}{j\beta a}\ \left\|\boldsymbol{\Gamma}'(x(\eta))\right\|e^{-j\ \beta a\ (\gamma(\eta_o)-\gamma(\eta))} \begin{pmatrix} w_i(a,\eta)\frac{A_i(a,\ \eta,\eta)}{\frac{d\Phi'(a,\ \eta_o,\eta)}{dx_o}|_{\eta_o=\ \eta}}\frac{e^{j\ \beta a\ (\eta_o\ -\eta)}}{(\eta_o-\eta)} - \\ w_i(-a,\eta)\frac{A_i(-a,\ \eta,\eta)}{\frac{d\Phi'(-a,\ \eta_o,\eta)}{dx_o}|_{\eta_o=\ \eta}}\frac{e^{-j\ \beta a\ (\eta_o\ -\eta)}}{(\eta_o-\eta)} \end{pmatrix} \tag{19}$$

Now, if the following choice of the weight function is performed

$$w_i(x',x(\eta)) = \frac{-\frac{d\Phi'(x',x_o(\eta_o),x(\eta))}{dx_o}|_{\eta_o=\eta}}{2\left\|\boldsymbol{\Gamma}'(x(\eta))\right\|A_i(x',x_o(\eta),x(\eta))} \tag{20}$$

all the amplitude terms in (20) depending only on η are exactly balanced and the kernel function can be rewritten as

$$K(\eta_o,\eta) \approx\ e^{-j\beta a(\gamma(\eta_o)-\gamma(\eta))}\ sinc(\beta a(\eta_o-\eta)) \tag{21}$$

Accordingly, the eigenvalue problem $TT^{\dagger}v_n = \sigma_n^2 v_n$ can be now expressed in the simple and nice form

$$\begin{aligned} &\int_{\eta(x_{min})}^{\eta(x_{max})} e^{-j\beta a(\gamma(\eta_o)-\gamma(\eta))}sinc(\beta a(\eta_o-\eta))v_n(\eta)d\eta \\ &= \sigma_n^2 v_n(\eta_o) \end{aligned} \tag{22}$$

In Appendix B, the expression of the weight function $w_i(x', \eta)$ is explicitly written both for a magnetic and an electric current. Moreover, it is shown that if $|x| \leq a$ and the observation curve $\boldsymbol{\Gamma}(x)$ satisfies condition (57) for the absence of stationary points then $w_i(x', x)$ is surely positive. Instead, if $|x| > a$ only the concave observation curves satisfying (57) ensure that $w_i(x', x) > 0$.

IV. NDF AND SAMPLING OF THE NEAR FIELD

In this section the NDF of the near field is analytically evaluated. In addition, a sampling representation of the near field employing a number of field samples equal to the NDF is provided. In order to find the NDF of the near field, the number of relevant eigenvalues of (22) must be computed. Fixing

$$\hat{v}_n(\eta_o) = e^{\ j\ \beta a\ \gamma(\eta_o)}\ v_n(\eta_o) \tag{23}$$

Equation (22) can be rewritten as

$$\int_{\eta_{max}}^{\eta_{min}} sinc(\beta a\ (\eta_o-\eta))\ \hat{v}_n(\eta)d\eta = \sigma_n^2\hat{v}_n(\eta_o) \tag{24}$$

where $\eta_{max} = \eta(x_{max})$ and $\eta_{min} = \eta(x_{min})$.

The eigenvalues of (24) have been studied by Slepian and Pollak in [52], where they have shown that the eigenvalues of a self-adjoint operator with a sinc kernel exhibit a step like behaviour with the knee occurring at the index

$$M = \left[\frac{\beta a}{\pi}(\eta_{max} - \eta_{min})\right] \tag{25}$$

with $[\cdot]$ denoting the integer part of the correspondent scalar. The scalar M provides an analytic evaluation of the NDF of the near field radiated by a magnetic or an electric current when it is observed over the curve $\boldsymbol{\Gamma}(x)$. From (25), it is evident that the NDF depends only on the wavenumber β and on some geometrical parameters like the source size $2a$ and the endpoints of the observation curve $(x_{max}, z(x_{max}))$

and $(x_{min}, z(x_{min}))$. Moreover, it is worth highlighting that the NDF expression can be seen as the product of the factors. The first factor $2\beta a/\pi$ represents the maximum value achievable by NDF of the field radiated by a strip source. Such a number is reached when the observation curve has an infinite extension along the $x-$ axis or subtend at least an angle of π.

The second factor $[\eta_{max} - \eta_{min}]/2$ takes into account that observation curve is truncated along the x direction or subtend an angle lower than π (in such cases the value of $[\eta_{max} - \eta_{min}]/2$ is always lower than 1).

Now, a sampling representation of the near field that exploits a number of field samples equal to the NDF is provided. On the basis of (24), it is possible to state that the eigenfunctions $\tilde{v}_n(\eta_o)$ are bandlimited functions with a bandwidth equal to βa. Accordingly, $\tilde{v}_n(\eta_o)$ can be represented with a good accuracy through the following truncated Shannon sampling series

$$\tilde{v}_n(\eta_o) = \sum_{m=0}^{M} \tilde{v}_n(\eta_{om})\ sinc[\beta a\ (\eta_o - \eta_{min}) - m\pi] \quad (26)$$

where

$$\eta_{om} = \eta_{min} + m\frac{\pi}{\beta a}\ \forall m \in \{0, 1, \ \ldots, \ M\} \quad (27)$$

Note that the index m is chosen in such a way that only the samples η_{om} falling into the set $[\eta_{min}, \eta_{max}]$ are considered.

By (23) and (26), the following sampling representation of $v_n(\eta_o)$ is obtained

$$v_n(\eta_o) = e^{-j\beta a\gamma(\eta_o)} \sum_{m=0}^{M} v_n(\eta_{om}) e^{j\beta a\gamma(\eta_{om})} sinc[\beta a(\eta_o - \eta_{min}) - m\pi] \quad (28)$$

Since the radiated field E can be represented through a linear combination of the eigenfunctions $\{v_n(\eta_o)\}$, it can be expressed by the following interpolating series

$$E(x_o) = e^{-j\beta a\gamma(x_o)} \sum_{m=0}^{M} E(x_{om}) e^{j\beta a\gamma(x_{om})} sinc[\beta a(\eta_o - \eta_{min}) - m\pi] \quad (29)$$

where $\forall m \in \{0, \ldots, M\}$ the sampling point x_{om} satisfies the equation $\eta(x_{om}) = \eta_{om}$. Hence, x_{om} is the solution of the equation

$$\frac{R(-a, x_{om}) - R(a, x_{om})}{2a} = \eta_{om} \quad (30)$$

which represents the equation of a hyperbola whose foci are the points $(0, -a)$ and $(0, a)$. Accordingly, Equation (30) can be also rewritten in the following form

$$\frac{x_{om}^2}{{\eta_{om}}^2} - \frac{z(x_{om})^2}{1 - {\eta_{om}}^2} = a^2 \quad (31)$$

The latter can be solved only after the observation curve $\mathbf{\Gamma}(x) = (x, z(x))$ has been specified.

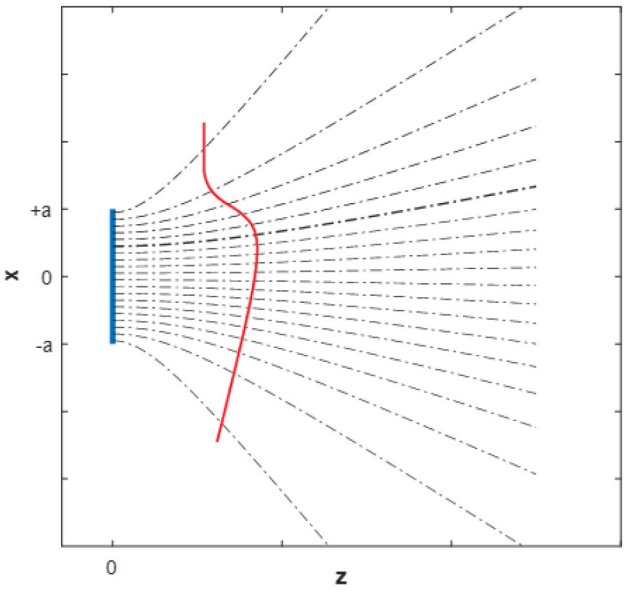

FIGURE 2. Pictorial view of the hyperbolas whose intersections with the observation curve returns the sampling points.

From the previous discussion, it is evident that the sampling points $\{x_{om}\}$ are the intersection between the observation curve $\Gamma(x)$ and the family of hyperbolas described by (30). A pictorial view of such hyperbolas is given in Fig. 2. Note that since the equation $\eta(x_{om}) = \eta_{om}$ is nonlinear, the uniform sampling step in η_o is mapped into a non-uniform sampling in the variable x_o. Accordingly, the field samples are non-uniformly arranged along the observation domain.

V. NUMERICAL RESULTS

In this section a numerical analysis is performed

1. to corroborate the analytical expression of the NDF provided by (25),
2. to validate the interpolation formula of the near field (29).

Such validation is performed by comparing the exact field computed by the radiation model (2) with the interpolation series (29). To establish the mismatch between the exact field and its approximation provided by (29), the relative error

$$err = \frac{||E - E_{exact}||}{||E_{exact}||} \quad (32)$$

is evaluated.

The analysis is developed with reference to different observation curves. Since the case of a line parallel to the source has been already examined in [34], [35]; here, at first, the case of an oblique line is considered. Then, the case of a circumference arc is examined.

A. AN OBLIQUE LINE

The configuration sketched in Fig. 3 is considered.

The source extends on the interval $[-a, a] = [-10\lambda, 10\lambda]$. The observation curve is the oblique line

$$z(x) = s_o \cdot x + z_o \quad (33)$$

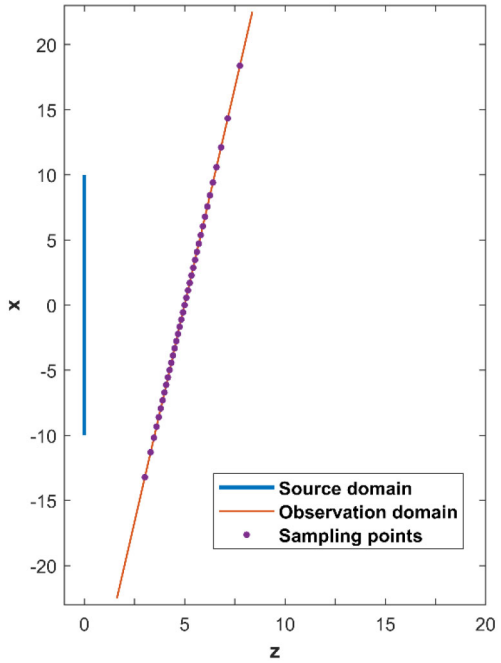

FIGURE 3. Strip source observed over an oblique line.

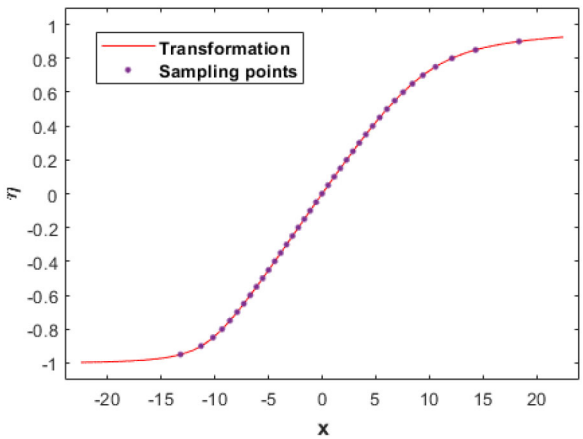

FIGURE 4. Diagram of the transformation $\eta = \eta(x)$.

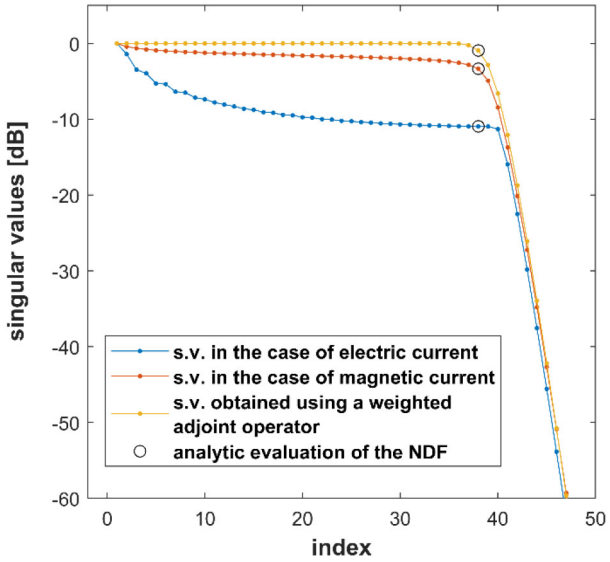

FIGURE 5. Comparison between the singular values of the radiation operator and the singular values obtained by introducing a weight function in the adjoint definition.

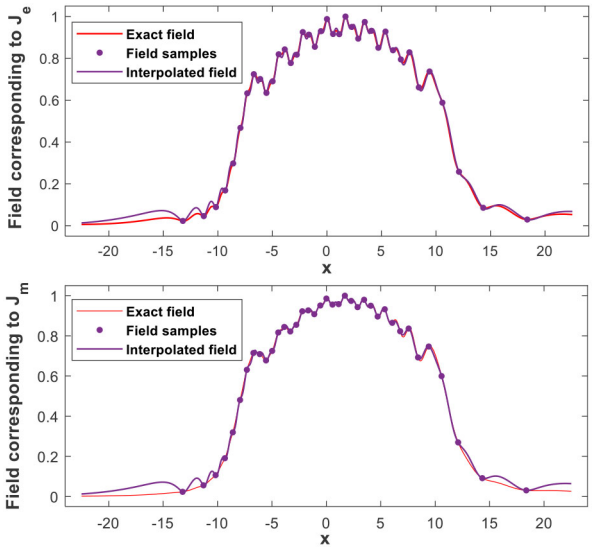

FIGURE 6. Comparison between the exact field and the interpolation provided by Equation (29).

with $s_o = 0.15$, $z_o = 5\lambda$, and $x \in OD = [-22.5\lambda, 22.5\lambda]$. Since the slope of the observation line satisfies condition (57), the evaluation of the kernel based only on the endpoints works well in the considered test case. In Fig. 4 the function $\eta(x)$ corresponding to the considered observation curve is shown. As can be seen from Fig. 4, in the present case, the trasformation is injective. Accordingly, the anlaysis by the variables (η_o, η) can be exploited to study the singular values of the radiation operator.

In Fig. 5 the singular values of the radiation operator both for an electric and a magnetic current are compared with the singular values obtained by introducing a weight function in the adjoint definition. From Fig. 5, it is evident that the singular values of the radiation operator and those obtained by introducing a weight function in the adjoint definition decay abruptly in correspondence of the same critical index M. For the considered configuration, such index is equal to 38 in perfect agreement with the analytical prevision provided by (25).

Now, the interpolation formula (29) is validated by a numerical analysis. For the considered configuration, the sampling points $\{x_{om}\}$ obtained by the solution of (31) are given by

$$x_{om} = \frac{\eta_{om}}{1 - {\eta_{om}}^2 - s_o^2 \eta_{om}^2} \times \left[s_o z_o \eta_{om} + \sqrt{1 - {\eta_{om}}^2} \sqrt{z_o^2 + a^2 \left(1 - {\eta_{om}}^2 - s_o^2 {\eta_{om}}^2\right)} \right] \tag{34}$$

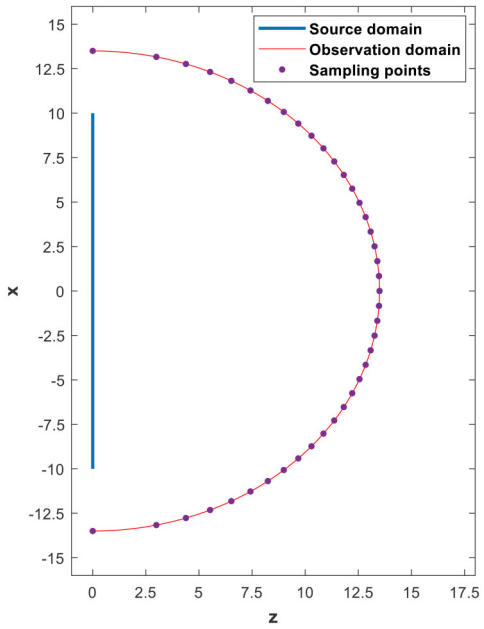

FIGURE 7. Strip source observed over a circumference arc.

In the numerical test, the field radiated by the source current

$$J_i(x') = 0.5\left[\cos\left(\frac{\pi}{2a}x'\right) + 1\right]e^{-j0.3\beta x'} \tag{35}$$

is considered. In particular, the exact field corresponding to $J_e(x')$ and $J_m(x')$ is compared with the approximation provided by (29) in Fig. 6.

As it can be appreciated from Fig. 6, the interpolated field overlaps well with the exact field despite the number of samples used for the interpolation is just equal to the NDF. In particular, it results that $err = 0.032$ in the case of electric current and $err = 0.044$ in the case of magnetic current.

B. AN ARC OF CIRCUMFERENCE

In this section, the field radiated by the same source considered in Section V-A is observed over an arc of circumference of radius $R_o = 13.5\lambda$ subtending the angular sector $[-89°, 89°]$. The geometry is sketched in Fig. 7.

The cartesian equation of the observation curve is

$$z(x) = \sqrt{R_o^2 - x^2} \tag{36}$$

Since angular extension of the observation arc is a little bit lower than a semi-circumference, condition (57) is fulfilled; hence, the asymptotic analysis based on the contributions of the endpoints can be applied. Moreover, also the transformation $\eta = \eta(x)$ is injective as it can be appreciated from Fig. 8.

As concerns the spectrum of the radiation operator, in Fig. 9 the singular values of the radiation operator both for an electric and a magnetic current are compared with the singular values obtained by introducing a weight function in the adjoint definition. The three diagrams shown in

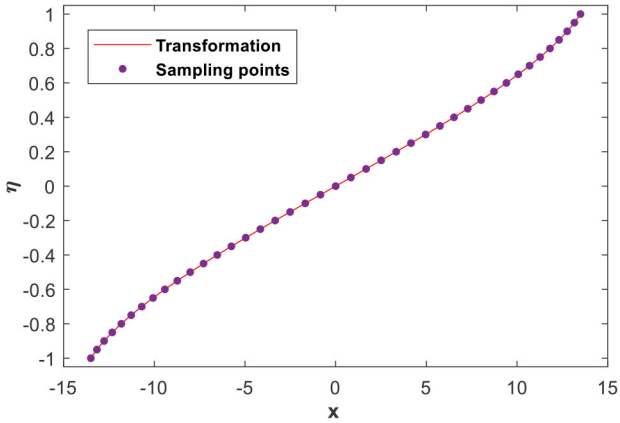

FIGURE 8. Behavior of the transformation $\eta = \eta(x)$.

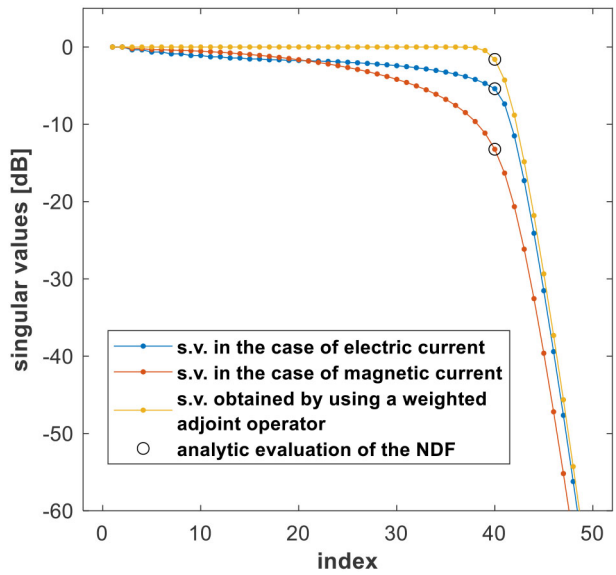

FIGURE 9. Comparison between the singular values of the radiation operator and the singular values obtained by introducing a weight function in the adjoint definition.

Fig. 9 exhibit the same number of relevant singular values. Such number is equal to 40 and it is well estimated by (25).

As concerns the sampling of the near field, the sampling points returned by (30) are

$$x_{om} = \eta_{om}\sqrt{a^2\left(1 - \eta_{om}{}^2\right) + R_o^2} \tag{37}$$

In Fig. 10, the exact field radiated by the electric and magnetic current in (35) is compared with the interpolated field provided by (29). Despite the number of field samples is only 41, the interpolated field matches well with the exact one; indeed, $err = 0.0061$ in the case of electric current and $err = 0.0244$ in the case of magnetic current.

VI. EXTENSION OF THE APPROACH TO THE NEAR FIELD INTENSITY

In this section, the approach developed above to evaluate the "essential" dimension of the near field is extended to the case

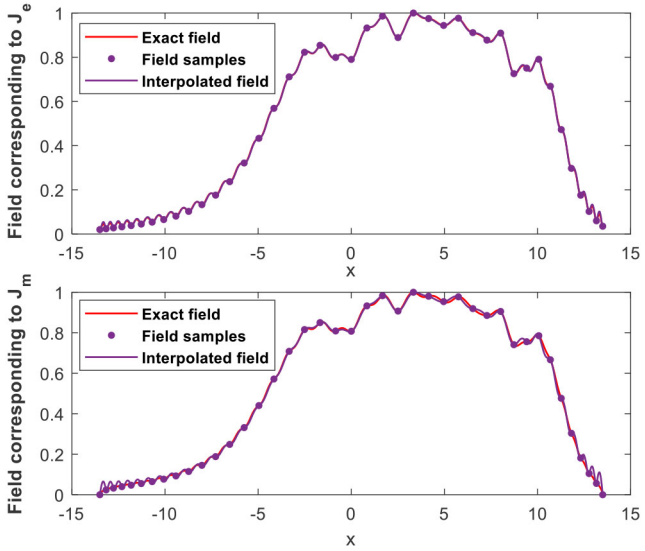

FIGURE 10. Comparison between the exact field and the interpolation provided by Equation (29).

of its intensity (i.e., the square amplitude). To achieve this goal, a linear representation of the quadratic problem

$$|E(x)|^2 = \left|T_i\ J_i(x')\right|^2 = \left|\int_{-a}^{a} g_i(x', x)\ J_i(x')dx'\right|^2 \quad (38)$$

is obtained by introducing the lifting operator. Then, the dimension of the field intensity is found by evaluating the number of relevant singular values of such an operator with the same strategy employed before for the radiation operator. Finally, an efficient sampling criterion of $|E|^2$ is shown.

With the aim to obtain a linear representation of $|E(x)|^2$, the quadratic model (38) can be rewritten as $|E(x)|^2 = T_i\ J_i(x')\ [T_i\ J_i(x'')]^*$ and a new unknown function $F(x', x'') = J_i(x')\ J_i^*(x'')$ can be introduced. Such redefinition of the unknown space allows recasting the quadratic model (38) into the linear model

$$|E(x)|^2 = L_i\ F(x', x'') \quad (39)$$

where the lifting operator

$$L_i : F(x', x'') \in L^2(SD\ \text{x}\ SD) \rightarrow |E(x)|^2 \in L_2^+(OD)$$

is defined as

$$L_i F_i = \int_{-a}^{a}\int_{-a}^{a} g_i(x', x)\ g_i^*(x'', x)\ F_i(x', x'')dx'dx'' \quad (40)$$

Accordingly, the corresponding adjoint operator is given by

$$L_i^\dagger |E|^2 = \int_{x_{min}}^{x_{max}} p_i(x', x'', x) g_i^*(x', x) g_i(x'', x)|E(x)|^2 \left\|\mathbf{\Gamma}'(x)\right\| dx \quad (41)$$

where $p_i(x', x'', x)$ represents the weight function. Since the singular values of L_i are the square root of the eigenvalues of $L_i L_i^\dagger$, the self-adjoint operator $L_i L_i^\dagger$ is now considered. It is defined as

$$L_i L_i^\dagger |E|^2 = \int_{x_{min}}^{x_{max}} H_i(x, x_o)|E(x)|^2 dx \quad (42)$$

where the kernel function $H_i(x_o, x)$ is given by

$$H_i(x_o, x) = \left\|\mathbf{\Gamma}'(x)\right\| \int_{-a}^{a}\int_{-a}^{a} p_i(x', x'', x) g_i(x', x_o)\ g_i^*(x'', x_o) g_i^*(x', x) g_i(x'', x)dx'dx'' \quad (43)$$

By assuming that the weight function can be factorized as $p_i(x', x'', x) = q_i(x', x) \cdot q_i(x'', x)$ and considering Eq. (5), (11) and (12), the kernel function can be rewritten as

$$H_i(x_o, x) = \left\|\mathbf{\Gamma}'(x)\right\| \left|\int_{-a}^{+a} q_i(x', x) A_i(x', x_o, x) e^{-j\beta a \Phi(x', x_o, x)} dx'\right|^2 \quad (44)$$

The integral in (44) is exactly the same as the integral in (10). Hence, if condition (57) for the absence of stationary point is satisfied, the kernel of $L_i L_i^\dagger$ can be evaluated with the same asymptotic approach shown in Section III. Accordingly, it can be recast as

$$H_i(\eta_o, \eta) \approx \frac{1}{(\beta a)^2}\left\|\mathbf{\Gamma}'(x(\eta))\right\| \frac{dx}{d\eta} \cdot \left| q_i(a, \eta) \frac{A_i(a, \eta, \eta)}{\frac{d\Phi'(a, \eta_o, \eta)}{dx_o} \frac{dx_o}{d\eta_o}|_{\eta_o=\eta}} \frac{e^{j\beta a(\eta_o - \eta)}}{(\eta_o - \eta)} - q_i(-a, \eta) \frac{A_i(-a, \eta, \eta)}{\frac{d\Phi'(-a, \eta_o, \eta)}{dx_o} \frac{dx_o}{d\eta_o}|_{\eta_o=\eta}} \frac{e^{-j\beta a(\eta_o - \eta)}}{(\eta_o - \eta)} \right|^2 \quad (45)$$

Equation (45) provides the kernel function after the asymptotic evaluation, the introduction of the variables (η_o, η), and the approximation of the amplitude terms.

As concerns the choice of $q_i(x', \eta)$, it is a little bit different from (20) since the square modulus appears in the last factor of (45). In particular, by choosing

$$q_i(x', \eta) = \frac{\frac{d\Phi(a, \eta_o, \eta)}{dx_o} \frac{dx_o}{d\eta_o}\Big|_{\eta_o=\eta}}{2\sqrt{\frac{dx}{d\eta}}\sqrt{\|\mathbf{\Gamma}'(x(\eta))\|} A_i(a, \eta, \eta)} \quad (46)$$

it follows that

$$H_i(\eta_o, \eta) \approx sinc^2(\beta a(\eta_o - \eta)) \quad (47)$$

Accordingly, the operator $L_i L_i^\dagger$ is well approximated by

$$L_i L_i^\dagger |E|^2 = \int_{\eta_{min}}^{\eta_{max}} sinc^2(\beta a(\eta_o - \eta))|E(\eta)|^2 d\eta \quad (48)$$

In order to evaluate the "essential" dimension of the space of the field intensity, the number of relevant eigenvalues of $L_i L_i^\dagger$ are now evaluated.

The latter was studied by Gori and Palma in [53], where they showed that the eigenvalues of a convolution operator with a sinc squared kernel exhibit a linear decay with the respect to the index. Hence, the eigenvalues are given by

$$\lambda_m\left(L_i L_i^\dagger\right) = \begin{cases} \frac{4\pi}{\beta a}\left(1 - \frac{m}{M}\right) & for\ m \le M \\ 0 & for\ m > M \end{cases} \quad (49)$$

where

$$M = \left\lceil \frac{2\beta a}{\pi}(\eta_{max} - \eta_{min}) \right\rceil \tag{50}$$

represents the number of eigenvalues of $L_i L_i^{\dagger}$ (or also the number of singular values of L_i) greater than zero. Hence, it can be taken as an analytic evaluation of the "essential" dimension of the space of the field intensity. Moreover, it represents also the minimum number of samples of $|E|^2$ required to sample it without loss of information.

At this juncture, the question of providing the optimal sampling point and an efficient sampling representation of $|E|^2$ is addressed. According to (48), the kernel of $L_i L_i^{\dagger}$ is a bandlimited function with respect to the variable η_o with a bandwidth equal to $2\beta a$. Hence, also the left singular functions of the lifting operator have the same bandwidth. This implies that they can be expressed by a Shannon sampling series. Moreover, since $|E|^2$ can be written as a linear combination of the first M left singular functions, also the field intensity can be expanded with a similar sampling series. Therefore, it results that

$$|E(x_o)|^2 = \sum_{m=0}^{M} \left|E\big(\eta(x_{om})\big)\right|^2 sinc\big(2\beta a\big(\eta(x_o) - \eta(x_{min})\big) - m\pi\big) \tag{51}$$

where

$$\eta(x_{om}) = \eta(x_{min}) + m\frac{\pi}{2\beta a} \forall m \in \{0, 1, \ldots, M\} \tag{52}$$

Note that, apart for the exponential terms appearing in (29), the main difference between the sampling expansion of the near-field and the correspondent expansion of the near-field intensity is the bandwidth of the sampling functions that doubles. Accordingly, the sampling step for the field intensity halves and number of sampling points doubles.

With the aim to corroborate, the validity of the field intensity representation provided by (51) the geometry in Fig. 7 is considered again. In Fig. 11 the exact field intensity corresponding to density current (35) is compared with its approximation provided by (51).

As can be seen from the Fig. 11, despite the number of field intensity samples is only equal to the dimension of the field intensity space ($M = 81$), the interpolated field intensity agrees very well with the exact field intensity. In particular, the relative error is $4.602 \cdot 10^{-4}$ in the case of electric current and it is equal to $2.615 \cdot 10^{-4}$ in the case of magnetic current.

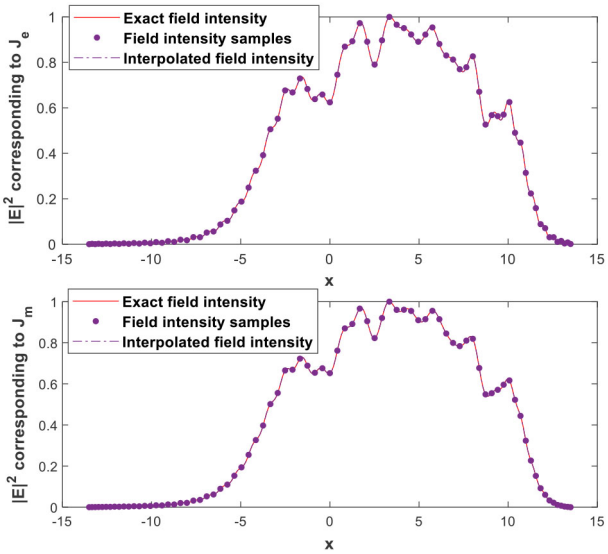

FIGURE 11. Comparison between the exact field intensity and the interpolation provided by Equation (51).

VII. CONCLUSION

In this paper, following the approach developed in [35] and [48] for the case of linear scanning, a sampling criterion of the near-field and its intensity which employs a non-redundant number of samples has been proposed for the case of a large class of smooth observation curves. More in detail, the minimum number of measurements and their locations required to sample the near-field and its intensity without loss of information have been analytically found.

Such goals have been achieved by studying the mathematical properties of radiation operator and of the correspondent lifting operator, respectively. In particular, the kernel of the eigenvalue problems involved in the computation of the singular values of such operators has been asymptotically evaluated by taking into account only of the endpoints of the source. Then, such kernel has been recast as convolution and bandlimited function by employing a change of variables. At this juncture, the minimum number of measurements required to well discretize the near field and its intensity has been computed by determining the number of relevant singular values of the radiation operator and the lifting operator, respectively. The optimal sampling positions for the field and its intensity have been found by considering the bandwidth of the left singular functions expressed in the new variable.

The main peculiarity of the proposed sampling criterion is its applicability to a large class of smooth observation curves. Only some issues can limit the applicability of the proposed approach. One of these is the presence of stationary points in the phase of the function that must be integrated to evaluate the kernel. However, as shown in Appendix A, no stationary points appears when all the possible straight lines linking two different point of the observation curve do not intersect the source. Instead, an interesting setup where the phase function admits a stationary point is analyzed in [54].

Another issue concerns the injectivity of the transformation $\eta(x)$, the positivity of the weight function (discussed in Appendix B), and the possible singularity in kernel introduced by the Jacobian term $dx/d\eta$ appearing in (17).

Despite the above-mentioned points, the proposed sampling method is suitable in several near field techniques both for the standard scanning (also in offset configuration)

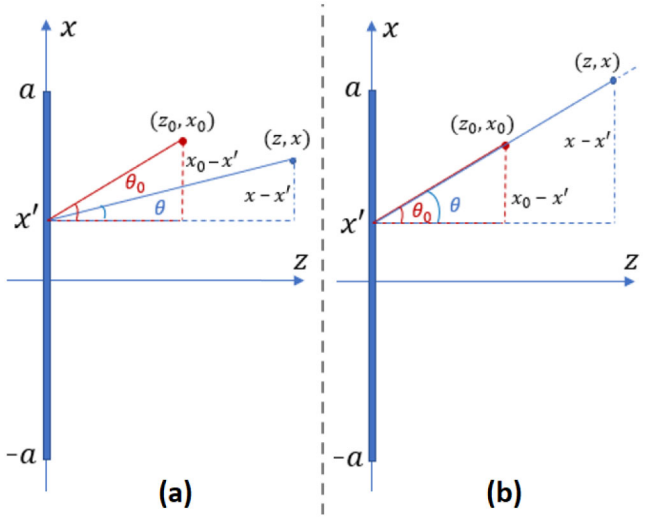

FIGURE 12. (a) Geometric representation of the angles θ_o and θ. (b) Pictorial view of the condition for which x' is a stationary point.

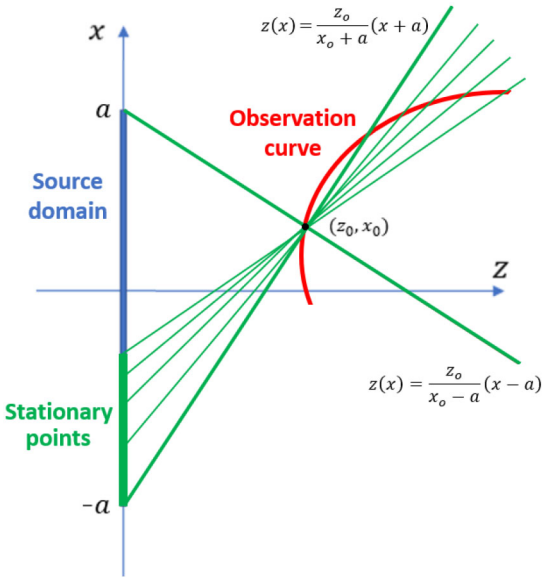

FIGURE 13. A configuration with stationary points in the phase function Φ.

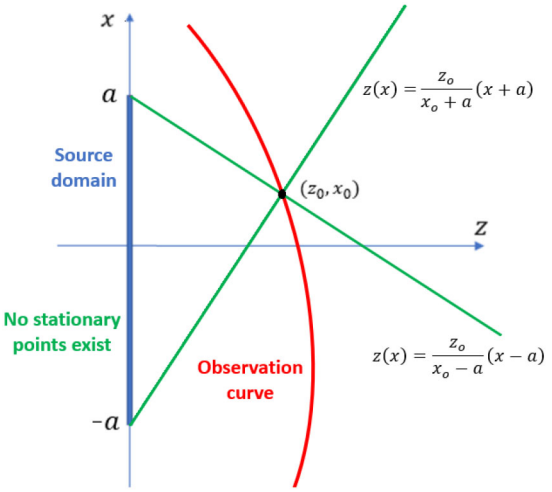

FIGURE 14. A configuration without stationary points in the phase function Φ.

and for a large set of unconventional observation curves that can be important also for UAV-mounted probes.

APPENDIX A
DISCUSSION ON THE EXISTENCE OF STATIONARY POINTS

In this Appendix the solution of the stationary condition

$$\Phi' = \frac{d\Phi}{dx'} = \frac{1}{a}\left(\frac{x - x'}{R(x', x)} - \frac{x_o - x'}{R(x', x_o)}\right) = 0 \qquad (53)$$

with respect to variable x' is discussed.

To solve Eq. (53), a geometric interpretation of the terms $(x-x')/R(x', x)$ and $(x_o-x')/R(x', x)$ can be exploited. From the diagram in Fig. 12a, it is evident that

$$\frac{x - x'}{R(x', x)} = sin\ \theta \quad \frac{x_o - x'}{R(x', x)} = sin\ \theta_o \qquad (54)$$

where θ_o and θ are respectively

- the angle between the axis $x = x'$ and the line linking the point $(0, x')$ to $(z(x_o), x_o)$;
- the angle among the axis $x = x'$ and the line linking the point $(0, x')$ to $(z(x), x)$.

On the basis of (54), the stationary condition (53) can be written as

$$sin\ \theta_o = sin\ \theta \qquad (55)$$

The latter is satisfied only if the source point $(0, x')$, and the points $(z(x_o), x_o)$ and $(z(x), x)$ of the observation curve $\Gamma(x)$ are aligned (see Fig. 12b). In such a case, x' represents the solution of (53) corresponding to the couple (x_o, x).

Therefore, it is possible to state that the solutions of (53) for a given x_o are represented by all the source points x' aligned with the point $(z(x_o), x_o)$ and another point of the observation curve $\mathbf{\Gamma}(x)$. In other words, the stationary points for a given x_o are all the source points x' that intersect the straight lines linking $(z(x_o), x_o)$ to other points of $\mathbf{\Gamma}(x)$ (see Fig. 13).

On the contrary, no stationary points exist when all the possible straight lines linking the point $(z(x_o), x_o)$ to other points $(z(x), x)$ of the observation curve do not intersect with the source (see Fig. 14). This happens if and only if the slope of such lines, i.e.,

$$\frac{\Delta z}{\Delta x} = \frac{z(x) - z(x_o)}{x - x_o}, \qquad (56)$$

is limited by the slopes of the lines linking the endpoints of the source to the point $(z(x_o), x_o)$. In particular, for the absence of stationary points, it must happen that

$$\frac{z(x_o)}{x_o - a} < \frac{\Delta z}{\Delta x} < \frac{z(x_o)}{x_o + a} \quad if\ |x_o| < a$$
$$\frac{\Delta z}{\Delta x} < \frac{z(x_o)}{x_o + a} \text{ or } \frac{\Delta z}{\Delta x} > \frac{z(x_o)}{x_o - a} \quad if\ |x_o| > a$$

$$\begin{aligned} \frac{\Delta z}{\Delta x} &< \frac{z(x_o)}{x_o + a} \ \ if \ |x_o| = a \\ \frac{\Delta z}{\Delta x} &> \frac{z(x_o)}{x_o - a} \ \ if \ |x_o| = -a \end{aligned} \tag{57}$$

for each $x \in [x_{min}, x_{max}] : \{x \neq x_o\}$.

Generalizing the previous discussion to the case where both x_o and x change, it is possible to conclude that the stationary condition $\Phi' = 0$ does not admit solution $\forall (x_o, x)$ such that $x_o \neq x$ if all the possible straight lines linking two generic points of the observation curve $\mathbf{\Gamma}$ do not intersect with the source. This happens if and only if (57) is fulfilled $\forall (x_o, x) \in [x_{min}, x_{max}] \times [x_{min}, x_{max}]$ such that $x_o \neq x$.

APPENDIX B
DETAILS ON THE WEIGHT FUNCTION

In this Appendix some useful details on the weight function

$$w_i(x', x) = \frac{-\frac{d\Phi'}{dx_o}|_{x_o = x}}{2\|\mathbf{\Gamma}'(x)\| A_i(x', x, x)} \tag{58}$$

are provided. In particular, its expression is first particularized in the case of magnetic and electric current. Later, some useful considerations on the sign of weight function are performed.

In order to write explicitly the weight function $w_i(x', x)$ in the case of magnetic and electric current, the derivative of Φ' with respect to x_o must be computed. The latter is given by

$$\frac{d\phi'}{dx_o} = -\frac{z(x_o)}{aR^3(x', x_o)} \left(z(x_o) - \frac{dz}{dx_o}(x_o - x') \right) \tag{59}$$

Now, taking into account that $\|\mathbf{\Gamma}'(x)\| = \sqrt{1 + [z'(x)]^2}$ and considering (11) and (59), the weight function can be rewritten as

$$w_i(x', x) = \begin{cases} \frac{4\pi}{\zeta^2 \beta a} \frac{z(x)\left(z(x) - \frac{dz}{dx}(x - x')\right)}{R^2(x', x)\sqrt{1 + \left(\frac{d}{dx} z(x)\right)^2}} & \text{for } i = e \\ \frac{4\pi}{\beta a} \frac{z(x) - \frac{dz}{dx}(x - x')}{z(x)\sqrt{1 + \left(\frac{d}{dx} z(x)\right)^2}} & \text{for } i = m \end{cases} \tag{60}$$

Equation (60) provides a closed form expression of the weight function that works until the approximation performed in (18) is true.

Let us note that if the observation curve is a line parallel to the source, the derivative appearing in (60) is zero. Hence, at least for a magnetic current, the weight function is a constant. In such a case, the kernel of $T_m T_m^{\dagger}$ is a sinc kernel of difference type also without the insertion of weight function in the adjoint operator definition. Hence, in such a particular case, it is possible to evaluate not only the number of relevant eigenvalues but also their value.

At this juncture, some useful considerations on the mathematical properties of weight function are performed. As stated in Section II, the weight function must be real and positive. Since all the terms appearing in (60) are real, the weight function is surely a real function.

As concerns the sign of w_i, the discussion is more intricate. From Equation (60), it can be observed that the sign of the weight function is determined by the difference

$$z(x) - \frac{dz}{dx}(x - x'). \tag{61}$$

Without any information on the observation curve, nothing can be said on the sign of the difference in (61) and, consequently, on the sign of the weight function. However, if the observation curve lies in the semi-plane $z > 0$ and satisfies condition (57) then $w_i(x', x)$ is positive $\forall (x', x)$ such that $-a \leq x' \leq a$ and for each $-a \leq x \leq a$.

In the regions $x < -a$ and $x > a$, the previous hypothesis on the observation curve are not sufficient to ensure the positivity of the weight function; however, if the observation curve lies in the semi-plane $z > 0$, satisfies condition (57), and it is also concave then the positivity of the weight function $w_i(x', x)$ is ensured also in the regions for which $x < -a$ and $x > a$.

Note that the fulfilment of (57) and the hypothesis of concavity of the observation curve imply that such curve satisfies the following constraints

$$\begin{cases} \frac{dz}{dx} > \frac{z(x)}{x - a} & \text{for } x < -a \\ \frac{dz}{dx} < \frac{z(x)}{x + a} & \text{for } x > +a \end{cases} \tag{62}$$

The proof of the positivity of $w_i(x', x)$ under the hypothesis that $z(x) > 0$ relies on the observation that the worst condition for the positivity of the weight function is when $\frac{dz}{dx}(x - x')$ attains its maximum; in particular, the weight function is positive until

$$max\left\{ \frac{dz}{dx}(x - x') \right\} < z(x) \tag{63}$$

Accordingly, in order to proof the positivity of $w_i(x', x)$ it is sufficient to observe that the fulfilment of (57) implies that the derivative term $\frac{dz}{dx}$ must satisfy the following constraint

$$\begin{aligned} &\frac{z(x)}{x - a} < \frac{dz}{dx} < \frac{z(x)}{x + a} \ for \ |x| < a \\ &\frac{dz}{dx} < \frac{z(x)}{x + a} \ \text{or} \ \frac{dz}{dx} > \frac{z(x)}{x - a} \ for \ |x| > a \\ &\frac{dz}{dx} < \frac{z(x)}{x + a} \ for \ x = a \\ &\frac{dz}{dx} > \frac{z(x)}{x - a} \ for \ x = -a \end{aligned} \tag{64}$$

Then, the maximum of $\frac{dz}{dx}(x - x')$ must be evaluated and compared with $z(x)$.

REFERENCES

[1] G. Giordanengo, M. Righero, F. Vipiana, G. Vecchi, and M. Sabbadini, "Fast antenna testing with reduced near field sampling," *IEEE Trans. Antennas Propag.*, vol. 62, no. 5, pp. 2501–2513, May 2014.

[2] M. A. Qureshi, C. H. Schmidt, and T. F. Eibert, "Efficient near-field far-field transformation for nonredundant sampling representation on arbitrary surfaces in near-field antenna measurements," *IEEE Trans. Antennas Propag.*, vol. 61, no. 4, pp. 2025–2033, Apr. 2013.

[3] M. Salucci, M. D. Migliore, P. Rocca, A. Polo, and A. Massa, "Reliable antenna measurements in a near-field cylindrical setup with a sparsity promoting approach," *IEEE Trans. Antennas Propag.*, vol. 68, no. 5, pp. 4143–4148, May 2020.
[4] N. Méziéres, M. Mattes, and B. Fuchs, "Antenna characterization from a small number of far-field measurements via reduced-order models," *IEEE Trans. Antennas Propag.*, vol. 70, no. 4, pp. 2422–2430, Apr. 2022, doi: 10.1109/TAP.2021.3118711.
[5] B. Fuchs, L. L. Coq, S. Rondineau, and M. D. Migliore, "Fast antenna far-field characterization via sparse spherical harmonic expansion," *IEEE Trans. Antennas Propag.*, vol. 65, no. 10, pp. 5503–5510, Oct. 2017.
[6] E. A. Marengo, A. J. Devaney, and R. W. Ziolkowski, "Inverse source problem and minimum-energy sources," *J. Opt. Soc. Amer. A*, vol. 17, no. 1, pp. 34–45, 2000.
[7] G. Wang, F. Ma, Y. Guo, and J. Li, "Solving the multi-frequency electromagnetic inverse source problem by the Fourier method," *J. Differ. Equ.*, vol. 265, no. 1, pp. 417–443, Jul. 2018.
[8] G. Schnattinger and T. F. Eibert, "Solution to the full vectorial 3-D inverse source problem by multilevel fast multipole method inspired hierarchical disaggregation," *IEEE Trans. Antennas Propag.*, vol. 60, no. 7, pp. 3325–3335, Jul. 2012.
[9] A. Kirkeby, M. T. R. Henriksen, and M. Karamehmedović, "Stability of the inverse source problem for the Helmholtz equation in R^3," *Inverse Problems*, vol. 36, no. 5, Apr. 2020, Art. no. 55007.
[10] M. A. Maisto, M. Masoodi, and R. Solimene, "Scattered field data collection in multi-static/multi-frequency radar imaging," in *Proc. IEEE ANTEM*, Winnipeg, MB, Canada, 2021, pp. 1–2.
[11] A. Capozzoli, C. Curcio, and A. Liseno, "Singular value optimization in inverse electromagnetic scattering," *IEEE Antennas Wireless Propag. Lett.*, vol. 16, pp. 1094–1097, 2017.
[12] R. Solimene, A. Brancaccio, R. Pierri, and F. Soldovieri, "TWI experimental results by a linear inverse scattering approach," *Progr. Electromagn. Res.*, vol. 91, pp. 259–272, Mar. 2009.
[13] A. Randazzo *et al.*, "A two-step inverse-scattering technique in variable-exponent Lebesgue spaces for through-the-wall microwave imaging: Experimental results," *IEEE Trans. Geosci. Remote Sens.*, vol. 59, no. 9, pp. 7189–7200, Sep. 2021.
[14] R. Solimene, M. A. Maisto, and R. Pierri, "Inverse source in the presence of a reflecting plane for the strip case," *J. Opt. Soc. Amer. A*, vol. 31, no. 12, pp. 2814–2820, 2014.
[15] O. M. Bucci and G. Franceschetti, "On the degrees of freedom of scattered fields," *IEEE Trans. Antennas Propag.*, vol. 37, no. 7, pp. 918–926, Jul. 1989.
[16] R. Solimene, M. A. Maisto, G. Romeo, and R. Pierri, "On the singular spectrum of the radiation operator for multiple and extended observation domains," *Int. J. Antennas Propag.*, vol. 2013, Jul. 2013, Art. no. 585238.
[17] G. Newsam and R. Barakat, "Essential dimension as a well-defined number of degrees of freedom of finite-convolution operators appearing in optics," *J. Opt. Soc. Amer. A*, vol. 2, no. 1, pp. 2040–2045, 1985.
[18] R. Piestun and D. A. B. Miller, "Electromagnetic degrees of freedom of an optical system," *J. Opt. Soc. Amer. A*, vol. 17, no. 5, pp. 892–902, 2000.
[19] E. Joy and D. Paris, "Spatial sampling and filtering in near-field measurements," *IEEE Trans. Antennas Propag.*, vol. TAP-20, no. 3, pp. 253–261, May 1972.
[20] W. Leach and D. Paris, "Probe compensated near-field measurements on a cylinder," *IEEE Trans. Antennas Propag.*, vol. TAP-21, no. 4, pp. 435–445, Jul. 1973.
[21] O. M. Bucci, C. Gennarelli, and C. Saverese, "Optimal Interpolation of radiated fields over a sphere," *IEEE Trans. Antennas Propag.*, vol. 39, no. 11, pp. 1633–1643, Nov. 1991.
[22] R. G. Yaccarino, L. I. Williams, and Y. Rahmat-Samii, "Linear spiral sampling for the bipolar planar near-field antenna measurement technique," *IEEE Trans. Antennas Propag.*, vol. 44, no. 7, pp. 1049–1051, Jul. 1996.
[23] O. M. Bucci, C. Gennarelli, and C. Savarese, "Representation of electromagnetic fields over arbitrary surfaces by a finite and nonredundant number of samples," *IEEE Trans. Antennas Propag.*, vol. 46, no. 3, pp. 351–359, Mar. 1998.
[24] S. Joshi and S. Boyd, "Sensor selection via convex optimization," *IEEE Trans. Signal Process.*, vol. 57, no. 2, pp. 451–462, Feb. 2009.
[25] M. A. Qureshi, C. H. Schmidt, and T. F. Eibert, "Adaptive sampling in spherical and cylindrical near-field antenna measurements," *IEEE Antennas Propag. Mag.*, vol. 55, no. 1, pp. 243–249, Feb. 2013.
[26] J. Ranieri, A. Chebira, and M. Vetterli, "Near-optimal sensor placement for linear inverse problems," *IEEE Trans. Signal Process.*, vol. 62, no. 5, pp. 1135–1146, Mar. 2014.
[27] C. Jiang, Y. C. Soh, and H. Li, "Sensor placement by maximal projection on minimum Eigenspace for linear inverse problems," *IEEE Trans. Signal Process.*, vol. 64, no. 21, pp. 5595–5610, Nov. 2016.
[28] B. Hofmann, O. Neitz, and T. Eibert, "On the minimum number of samples for sparse recovery in spherical antenna near-field measurements," *IEEE Trans. Antennas Propag.*, vol. 67, no. 12, pp. 7597–7610, Dec. 2019.
[29] A. Capozzoli, C. Curcio, and A. Liseno, "On the optimal field sensing in near-field characterization," *Sensors*, vol. 21, no. 13, p. 4460, 2021.
[30] F. D'Agostino, F. Ferrara, C. Gennarelli, R. Guerriero, M. Migliozzi, and G. Riccio, "A useful sampling representation for mapping the antenna near-field," *IEEE Open J. Antennas Propag.*, vol. 2, pp. 709–717, 2021.
[31] R. R. Alavi, R. Mirzavand, A. Kiaee, and P. Mousavi, "An adaptive data acquisition technique to enhance the speed of near-field antenna measurement," *IEEE Trans. Antennas Propag.*, early access, Jan. 28, 2022, doi: 10.1109/TAP.2022.3145452.
[32] M. D. Migliore, "Horse (electromagnetics) is more important than horseman (information) for wireless transmission," *IEEE Trans. Antennas Propag.*, vol. 67, no. 4, pp. 2046–2055, Apr. 2019.
[33] H. R. Behjoo, A. Pirhadi, and R. Asvadi, "Optimal sampling in spherical near-field antenna measurements by utilizing the information content of spherical wave harmonics," *IEEE Trans. Antennas Propag.*, early access, Dec. 28, 2021, doi: 10.1109/TAP.2021.3137194.
[34] R. Solimene, M. A. Maisto, and R. Pierri, "Sampling approach for singular system computation of a radiation operator," *J. Opt. Soc. Amer. A*, vol 36, no. 3, pp. 353–361, 2019.
[35] R. Pierri and R. Moretta, "Asymptotic study of the radiation operator for the strip current in near zone," *Electronics*, vol. 9, no. 6, p. 911, 2020.
[36] K. Khare and N. George, "Sampling theory approach to prolate spheroidal wavefunctions," *J. Phys. A, Math. Gen.*, vol. 36, no. 39, 2003, Art. no. 10011.
[37] L. J. Foged, F. Saccardi, F. Mioc, and P. O. Iversen, "Spherical near field offset measurements using downsampled acquisition and advanced NF/FF transformation algorithm," in *Proc. IEEE EuCAP*, Davos, Switzerland, 2016, pp. 1–3.
[38] G. Virone *et al.*, "Antenna pattern verification system based on a micro unmanned aerial vehicle (UAV)," *IEEE Antennas Wireless Propag. Lett.*, vol. 13, pp. 169–172, 2014.
[39] T. Fritzel, R. Strauß, H.-J. Steiner, C. Eisner, and T. Eibert, "Introduction into an UAV-based near-field system for *in situ* and large-scale antenna measurements," in *Proc. IEEE CAMA*, Syracuse, NY, USA, 2016, pp. 1–3.
[40] M. García-Fernández *et al.*, "Antenna diagnostics and characterization using unmanned aerial vehicles," *IEEE Access*, vol. 5, pp. 23563–23575, 2017.
[41] F. R. Varela, J. F. Álvarez, B. G. Iragüen, M. S. Castañer, and O. Breinbjerg, "Numerical and experimental investigation of phaseless spherical near-field antenna measurements," *IEEE Trans. Antennas Propag.*, vol. 69, no. 12, pp. 8830–8841, Dec. 2021.
[42] A. Paulus, J. Knapp, and T. F. Eibert, "Phaseless near-field far-field transformation utilizing combinations of probe signals," *IEEE Trans. Antennas Propag.*, vol. 65, no. 10, pp. 5492–5502, Oct. 2017.
[43] A. Guth, C. Culotta-López, J. Maly, H. Rauhut, and D. Heberling, "Polyhedral sampling structures for phaseless spherical near-field antenna measurements," in *Proc. IEEE AMTA*, Newport, RI, USA, 2020, pp. 1–6.
[44] A. F. Morabito, R. Palmeri, V. A. Morabito, A. R. Laganà, and T. Isernia, "Single-surface phaseless characterization of antennas via hierarchically ordered optimizations," *IEEE Trans. Antennas Propag.*, vol. 67, no. 1, pp. 461–474, Jan. 2019.
[45] F. R. Varela, B. G. Iraguen, M. S. Castañer, J. F. Alvárez, M. Mattes, and O. Breinbjerg, "Combination of spherical and planar scanning for phaseless near-field antenna measurements," in *Proc. IEEE AMTA*, San Diego, CA, USA, 2019, pp. 1–6.

[46] T. Isernia, G. Leone, and R. Pierri, "Radiation pattern evaluation from near-field intensities on planes," *IEEE Trans. Antennas Propag.*, vol. 44, no. 5, p. 701, May 1996.
[47] R. Pierri and R. Moretta, "On data increasing in phase retrieval via quadratic inversion: Flattening manifold and local minima," *IEEE Trans. Antennas Propag.*, vol. 68, no. 12, pp. 8104–8113, Dec. 2020.
[48] R. Pierri, G. Leone, and R. Moretta, "The dimension of phaseless near-field data by asymptotic investigation of the lifting operator," *Electronics*, vol. 10, no. 14, p. 1658, 2021.
[49] E. Hille and J. D. Tamarkin, "On the characteristic values of linear integral equation," *Acta Math.*, vol. 57, no. 1, pp. 1–76, 1931.
[50] M. A. Maisto, R. Solimene, and R. Pierri, "Depth resolution in strip current reconstructions in near non-reactive zone," *J. Opt. Soc. Amer. A*, vol. 36, no. 6, pp. 975–982, 2019.
[51] M. Bertero and P. Boccacci, "Computation of the singular system for a class of integral operators related to data inversion in confocal microscopy," *Inverse Problems*, vol. 5, no. 6, p. 935, 1989.
[52] D. Slepian and H. O. Pollak, "Prolate spheroidal wave functions, Fourier analysis and uncertainty—I," *Bell Syst. Techn. J.*, vol. 40, no. 1, pp. 43–63, Jan. 1961.
[53] F. Gori and C. Palma, "On the Eigenvalues of the sinc^2 kernel," *J. Phys. A, Math. Gen.*, vol. 8, no. 11, p. 1709, 1975.
[54] R. Pierri and R. Moretta, "NDF of the near-zone field on a line perpendicular to the source," *IEEE Access*, vol. 9, pp. 91649–91660, 2021.

GIOVANNI LEONE (Member, IEEE) received the Laurea degree in electronic engineering from the University of Naples Federico II, Naples, Italy, in 1981.

From 1986 to 1992, he was an Associate Researcher of Electromagnetics with the University of Salerno, Italy. From 1992 to 2000, he was an Associate Professor with the University of Salerno and the Seconda Universitá degli Studi di Napoli, Italy. He is currently a Full Professor with the University of Campania Luigi Vanvitelli, Italy. He was responsible for research funding from the Italian Space Agency, Rome, Italy, the National Research Council, and the Ministry of Scientific Research. His current research interests include antenna measurement techniques and synthesis, phase retrieval of radiated fields, inverse scattering for non-destructive diagnostics, microwave tomography for subsurface sensing, and conformal antennas diagnostics.

RAFFAELE MORETTA (Member, IEEE) received the Laurea degree *(summa cum laude)* in electronic engineering and the Ph.D. degree in electronic and computer science engineering from the University of Campania "Luigi Vanvitelli" in 2018 and 2022, respectively.

Since 2016, he has started a scientific cooperation with the Electromagnetic Fields Group, University of Campania "Luigi Vanvitelli," where he is currently a Postdoctoral Researcher. His current research interests include inverse problems in electromagnetics with particular attention to phase retrieval, near field measurement techniques, and conformal antenna diagnostics.

Dr. Moretta is a member of the Italian Society of Electromagnetism. Moreover, in February 2021, he was under consideration by the committee of the IEEE Antennas Propagation Society for the R.W.P. King Award 2020.

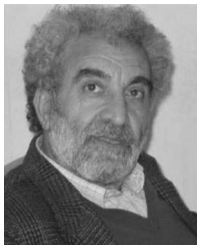

ROCCO PIERRI received the Laurea degree *(summa cum laude)* in electronic engineering from the University of Naples "Federico II" in 1976.

He was a Visiting Scholar with the University of Illinois at Urbana–Champaign, Urbana, IL, USA; Harvard University, Cambridge, MA, USA; Northeastern University, Boston, MA, USA; Supelec, Paris, France; and the University of Leeds, Leeds, U.K. He also extensively lectured abroad in many universities and research centers. He is currently a Full Professor with the University of Campania "Luigi Vanvitelli," Aversa, Italy. His current research interests include antennas, phase retrieval, near-field techniques, inverse electromagnetic scattering, subsurface sensing, electromagnetic diagnostics, microwave tomography, inverse source problems, and information content of radiated field.

Prof. Pierri was a recipient of the 1999 Honorable Mention for the H. A. Wheeler Applications Prize Paper Award of the IEEE Antennas and Propagation Society.